Wind Tunnel Testing of Active Flow Control on High-Lift Common Research Model

John C. Lin*, Latunia P. Melton†, Judith A. Hannon‡, Marlyn Y. Andino§,
Mehti Koklu**, Keith B. Paschal††, and Veer N. Vatsa‡‡

NASA Langley Research Center, Hampton, VA, 23681, USA

A 10%-scale high-lift version of the Common Research Model (CRM-HL) and an Active Flow Control (AFC) version of the model equipped with a simple-hinged flap (CRM-SHL-AFC) were successfully tested. The tests were performed in the 14- by 22-Foot Subsonic Tunnel (14x22) at the NASA Langley Research Center (LaRC). The CRM-HL has a set of 37° inboard and outboard single-element Fowler flaps. The CRM-SHL-AFC has a set of 50° inboard and 55° outboard simple-hinged flaps equipped with integrated modular AFC cartridges on the flap shoulder. Both high-lift configurations share the same 30° slats and engine nacelle. Three new types of AFC devices were examined: the Double-Row Sweeping Jets (DRSWJ), the Alternating Pulsed Jets (APJ), and the High Efficiency Low Power (HELP) actuators. The DRSWJ and the APJ actuators used two rows of unsteady jets, whereas the HELP actuators used a combination of unsteady and steady jets, to overcome strong adverse pressure gradients while minimizing the mass flow usage. Nozzle pressure ratio, mass flow consumption and the power coefficient, which takes account of both supply air pressure and mass flow usage for the actuators, were used for judging the performance efficiency of the AFC devices. A prestall lift performance degradation for the CRM-HL configuration was resolved with a properly placed nacelle chine. The configuration with nacelle chine was chosen as the representative reference conventional high-lift case for comparison with the CRM-SHL-AFC. The AFC-induced lift coefficient increment (ΔC_L) was maintained for the entire lift curve over the CRM-SHL-AFC case with no AFC for almost all flow-control cases examined. The lift curve of the reference CRM-HL have a slightly steeper slope compared to those of the CRM-SHL-AFC configurations. The HELP actuation concept was extremely effective in controlling flow separation in the "linear region" of the curves comparing lift coefficient to mass flow rate. The HELP actuation achieved a targeted ΔC_L of 0.50 using a moderate amount of mass flow and supply air pressure. The CRM-SHL-AFC configuration equipped with HELP actuation was able to match or exceed the lift performance of the reference conventional high-lift configuration (i.e., CRM-HL equipped with a nacelle chine), thus meeting the NASA Advanced Air Transport Technology (AATT) project goal.

I. Nomenclature

A_n	=	total area of all active nozzle exits
C_D	=	drag coefficient; (drag force)/($S \cdot q_\infty$)
C_L	=	lift coefficient; (lift force)/($S \cdot q_\infty$)
C_m	=	pitching moment coefficient; (pitching moment)/($S \cdot c_r \cdot q_\infty$), where c_r = 27.58 inches
C_p	=	pressure coefficient; $(p - p_\infty)/q_\infty$
C_Q	=	mass flow coefficient; $\dot{m}/(\rho_\infty \cdot S \cdot U_\infty)$
C_μ	=	momentum coefficient; $\dot{m}^2/(\rho_n \cdot A_n \cdot q_\infty \cdot S)$
C_π	=	power coefficient; $(C_Q \cdot P_a)/q_\infty$

* Senior Research Scientist, Flow Physics and Control Branch, MS 170, AIAA Associate Fellow
† Senior Research Scientist, Flow Physics and Control Branch, MS 170, AIAA Associate Fellow
‡ Senior Research Scientist, Flow Physics and Control Branch, MS 170
§ Research Scientist, Flow Physics and Control Branch, MS 170, AIAA Senior Member
** Research Scientist, Flow Physics and Control Branch, MS 170
†† Research Scientist, Flow Physics and Control Branch, MS 170
‡‡ Senior Research Scientist, Computation AeroSciences Branch, MS 128, AIAA Associate Fellow

M_∞	=	freestream Mach number
$\dot{m}$	=	total mass flow rate
p	=	pressure
p_∞	=	freestream static pressure
P_a	=	actuator plenum pressure
q_∞	=	freestream dynamic pressure
Re_{mac}	=	Reynolds number based on mean aerodynamic chord
S	=	wing reference area
U_∞	=	freestream velocity
x, y, z	=	coordinates along the model's longitudinal axis, lateral axis, and normal axis, respectively
α	=	angle of attack
ΔC_L	=	lift coefficient increment
ρ_∞	=	freestream density
ρ_n	=	air density at the actuator nozzle

II. Introduction

THE sizing, economics, and safety of modern transport aircraft are strongly influenced by the high-lift systems for takeoff and landing operations [1]. The NASA Advanced Air Transport Technology (AATT) Project is exploring the possibility of using Active Flow Control (AFC) [2,3] to provide the required lift performance while reducing the cruise drag associated with the external mechanisms used to deploy a slotted flap during high-lift operations [4-6]. System integration studies indicated that up to a 2.25% fuel burn reduction is possible if an AFC-enabled simplified high-lift system (i.e., simple-hinged flaps inboard and outboard) could provide the necessary lift recovery at the approach angle of attack [5]. The AFC-related performance gains are primarily due to the 3.3-count excrescence drag reduction obtained by the removal of the external fairings for the Fowler flap mechanism (see Fig. 1(a) for a typical example [7]). However, the main challenge is to develop an AFC system that can provide the necessary lift recovery on a simple-hinged flap high-lift system (Fig. 1(b)) while minimizing its pneumatic power requirement. Wind tunnel testing of AFC-enabled high-lift systems was performed as part of the AATT Project goals to reduce fuel burn for modern civil transport aircraft.

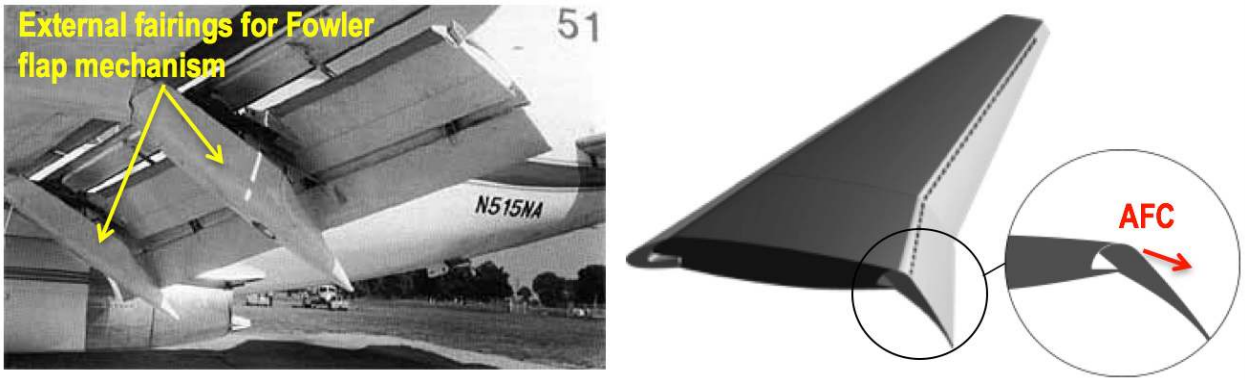

(a) An example of external fairings for Fowler flap mechanism.[7]

(b) A simple-hinged flap high-lift wing with AFC (no external fairings).

Fig. 1 Concept of AFC-enabled high-lift system for drag reduction.

The current high-lift research effort involves both conventional and AFC-enabled high-lift configurations that are based on the "open" NASA Common Research Model (CRM) [8,9]. The conventional high-lift configuration (CRM-HL), as reported by Lacy and Sclafani [10], is intended to be open as well. An AFC-enabled high-lift configuration (CRM-SHL-AFC) equipped with 50° inboard and 55° outboard (50°/55°) simple-hinged flaps was also built for wind-tunnel testing [11]. The outboard flap deflection was higher but necessary to align the outboard edge of the inboard flap with that of the inboard edge of the outboard flap. The 30° slat and most of the main wing, with the exception of the trailing edge/cove components, are the same between the AFC-enabled high-lift configuration and the conventional high-lift geometry. By keeping the conventional slat, the expectation is that the maximum lift should not change significantly.

Flow control is the ability to actively or passively manipulate a flow field to a desired state [12], and it has become a rapidly growing field in applied fluid dynamics because of its potential to dramatically improve system performance. AFC has been proposed to achieve the high-lift aerodynamic performance enhancement while reducing the system part count and associated external drag [4,5,11]. Steady blowing through slots as well as AFC actuators — such as synthetic jet actuators, fluidic oscillators, plasma actuators etc. — have been proposed in the literature [3]. The synthetic jet and plasma actuators are operated by electric power and have been examined for low to moderate adverse pressure gradients due to their limited flow control authority.

Steady blowing and fluidic oscillators (often referred to as sweeping jet actuators) use pneumatic power and have been successfully used in various flow control configurations. For example, steady blowing from the two dimensional slot at the flap shoulders (often referred to as circulation control or CC) has proven to be effective on a high-lift wing [13,14] that was designated as the Fundamental Aerodynamic Subsonic Transonic-Modular Active Control (FAST-MAC) model. A CC system using steady slot blowing can usually provide the necessary lift required for airfoils or wings with high flap deflections. However, one drawback of a steady blowing CC system is that it may require more pneumatic power (combination of mass flow and pressure) than what realistically can be implemented on an aircraft from a system integration stand point (e.g., excess weight penalty).

An unsteady version of the CC slot blowing was demonstrated on a high-lift (2D) airfoil with a highly deflected 65° flap in a water tunnel [15]. For this AFC methodology, unsteady fluctuations, generated by electronic valves, are superimposed on the steady blowing to control the separation behind the highly deflected flap. However, the unsteady CC was performed in a water tunnel with a 2D model. Therefore, the lift increment is expected to be reduced if the unsteady CC is applied to a 3D wing in air under compressible conditions.

It has been shown that unsteady AFC is more beneficial for optimal performance because it requires less mass flow input while satisfying the output requirements [2]. Sweeping jet actuators are a type of unsteady fluidic oscillator that have been shown to be reliable and efficient flow-control devices both in wind tunnel [16-24] and flight [25] tests. High Reynolds number wind tunnel tests [13] with AFC on the FAST-MAC model proved the effectiveness of the sweeping jet actuators, which produced a 54.7% reduction in mass flow usage at $\Delta C_L \approx 0.4$ compared to the steady CC blowing (see Figure 2).

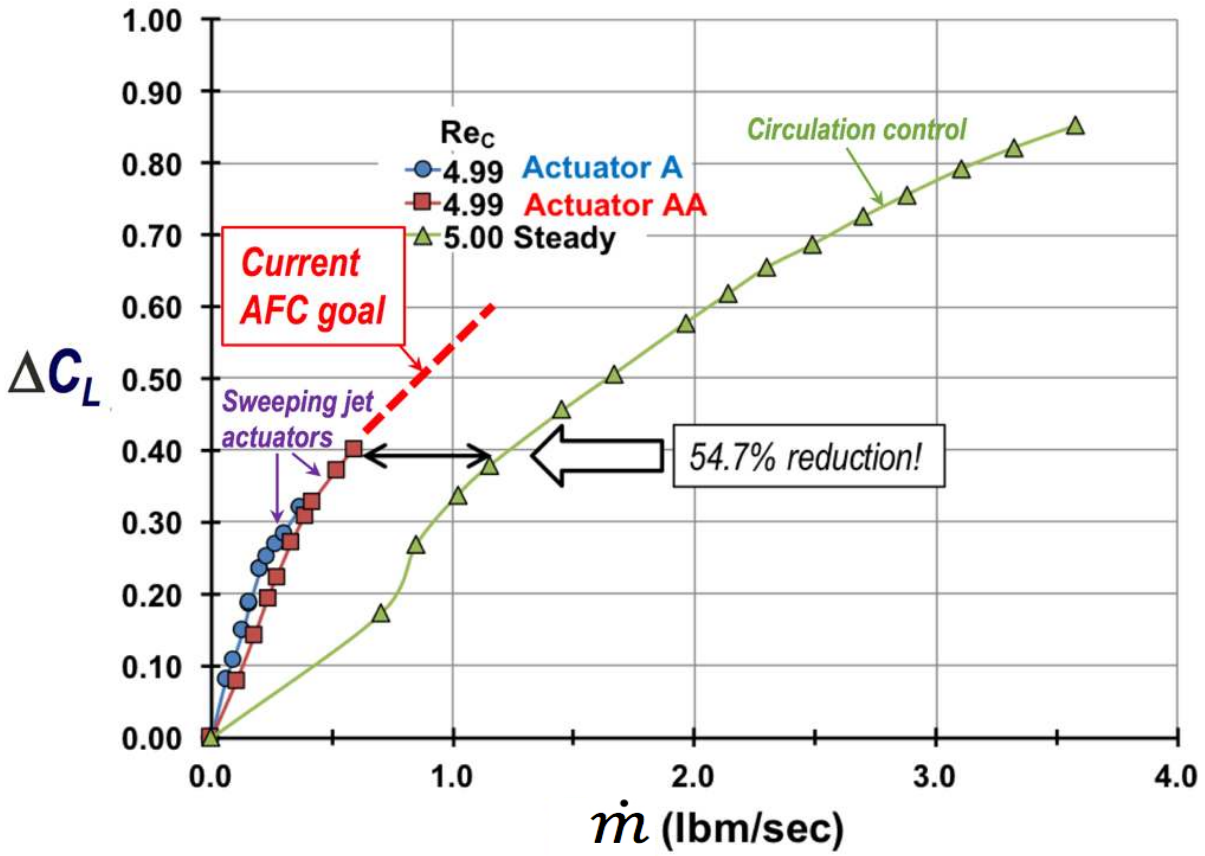

Fig. 2 Increase in lift coefficient (ΔC_L) versus the mass flow rate from Fig. 23 of Jones at al. [13] and the current AFC goal.

An improved sweeping jet actuation methodology was proposed in the form of utilizing three spanwise rows of fluidic oscillator arrays on a single-element high-lift airfoil (2D) with a 40° flap deflection [26]. The test was performed over a section of the 2D span of a model having a 35% model flap chord. However, it was uncertain whether this methodology could achieve the desired lift enhancement ($\Delta C_L \approx 0.5$) for simple-hinged flaps on a more complex, swept wing (3D) geometry with even larger deflections (> 40°) and thus higher adverse pressure gradients. Subsequently, a similar AFC methodology (i.e., multiple rows of sweeping jet actuators) was investigated numerically by Vatsa et al. [27] on the CRM-SHL-AFC. The CFD study indicated that AFC could only achieve a maximum ΔC_L of approximately 0.22, which is significantly less than that of a conventional CRM-HL configuration (i.e., the lift enhancement goal of $\Delta C_L \approx 0.5$).

Another low-power methodology for AFC is the traverse actuation as reported in Shmilovich et al. [6], where the AFC actuation was applied on the CRM-SHL-AFC. Although the traverse actuation is a novel approach to reduce the mass flow required, it produced a $\Delta C_L \approx 0.26$, which is only about half of the lift enhancement goal. Furthermore, electrically powered AFC systems such as plasma actuators or synthetic jet actuators that are currently available have limited control authority for highly deflected flaps.

Since the ΔC_L produced by the sweeping jet actuators (Actuators A and AA in Fig. 2) peaks at ~0.4, there is a strong motivation to extend the effective flow control range into the "linear region" of ΔC_L versus the mass flow rate curves. An AFC solution that could increase ΔC_L using modest mass flow rates (shown as the red dotted line) would meet the lift enhancement goal and be considered highly efficient. In the current study, innovative low-power AFC concepts using two rows of actuators were applied near the shoulder region of a highly-deflected simple-hinged flap to control flow separation and determine if a similar level of lift performance as that of the CRM-HL [10] in the landing configuration could be achieved on the CRM-SHL-AFC [11] with minimal pneumatic power consumption.

III. Wind Tunnel Test

The wind tunnel test was performed at the NASA LaRC 14- by 22-Foot Subsonic Tunnel (14x22) [28]. The 14x22 is an atmospheric, closed return wind tunnel with a 14.5-ft high, 21.75-ft wide, and 50-ft long test section. When testing in the closed-wall configuration, a maximum freestream velocity of 338 ft/s and a dynamic pressure (q_∞) of 144 psf could be achieved. The unit Reynolds number ranges from 0 to 2.2×10^6 per foot. A 10%-scale semispan (right wing) CRM-HL was fabricated and tested in the landing configuration at a nominal freestream Mach number (M_∞) of 0.2 and a corresponding q_∞ of approximately 60 psf.

The experimental measurements included forces and moments using a balance (NASA MC-110), surface static pressures using pressure taps and electronically scanned pressure (ESP) modules, surface dynamic pressures using unsteady pressure sensors, model deflection using videogrammetry, and flow visualization using minitufts. Based on the balance accuracy, angle of attack (α) and q_∞, the expected instrumentation uncertainty is estimated to be within ±0.01 for the lift coefficient (C_L), ±0.0030 to ±0.0040 for the drag coefficient (C_D), and ±0.0030 to ±0.0035 for the pitching moment coefficient (C_m). The uncertainty of the latter two is also a function of α — i.e., a greater uncertainty is associated with higher angles of attack. All data presented in this paper are without wall corrections applied.

A. Model Features

The main components of the half-body model are a semispan wing, a nacelle/pylon, and a semispan fuselage. Key model components such as the slat, wing under slat surface (WUSS), spoiler, and flap are all modular and replaceable. Provisions were also made for interchangeable model pieces for regions at the flap and slat side edges, wingtip, and aileron. The engine nacelle/pylon is removable to permit testing with a bare wing.

A photo and sketches of the CRM-HL in the 14x22 are shown in Fig. 3. The 10%-scale semispan model is installed on top of a 0.29 foot (~3.5 inches) peniche (or standoff), and as a result, the model and its peniche cover 68% of the tunnel span in the vertical direction. The model fuselage is 20.59 feet in length; therefore, it extends past the turntable and past the end of the model cart. The peniche is nonmetric and attached to the turntable, whereas the fuselage is metric and connected to the force balance below the model. A labyrinth seal provided the interface between the fuselage and the peniche.

Key model geometric reference parameters used for computing force and moment coefficients are:

- Mean aerodynamic chord (MAC) = 27.58 inches at y = 46.875 inches
- Wing semispan = 115.675 inches
- Reference area of the semispan model (S) = 2,973.6 in^2
- Moment reference center (MRC): x = 132.59 inches, y = 0 inches, z = 17.795 inches
- Based on MAC, $Re_{mac} \approx 3.27\times10^6$ for the landing configuration at $M_\infty = 0.20$

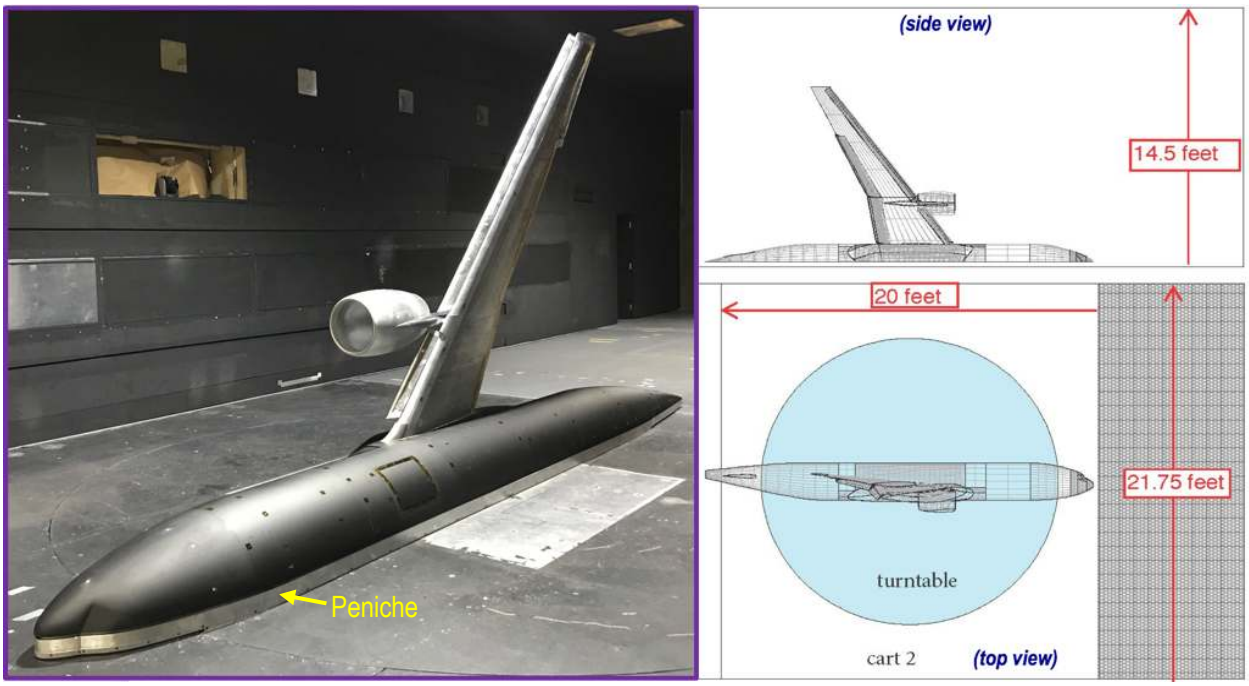

Fig. 3 Semispan CRM-HL in the 14x22

A schematic of the pressure tap locations, indicated by dots, is shown in Fig. 4. Most of the pressure taps are in streamwise arrays at eight spanwise locations with three rows across the inboard flap span, three rows across the outboard flap span, and two rows across the aileron region (i.e., y = 17.45, 27.75, 38.05, 48.35, 63.8, 79.25, 94.7, and 105 inches; where the yehudi break that separates the inboard and outboard flaps is located at y = 42.8 inches). Additionally, six spanwise arrays are on the upper wing surface with one row on the slat, three rows on the main wing, and two rows on the flap. The total number of pressure taps on the wing is 611. Other locations for pressure taps include the fuselage (56) and nacelle/pylon (63). There are thirty-one unsteady pressure sensors installed on the model that include six on the wingtip, seven on the pylon, six on the outboard edge of the conventional flap, and twelve on the simple-hinged flap (six each on the inboard and the outboard flaps).

The model spar is hollow to allow for routing of instrumentation and AFC plumbing. As mentioned previously, the model is capable of being tested with and without the engine nacelle. A filler piece connects the inboard and outboard slats when the nacelle is not installed to provide a continuous slat.

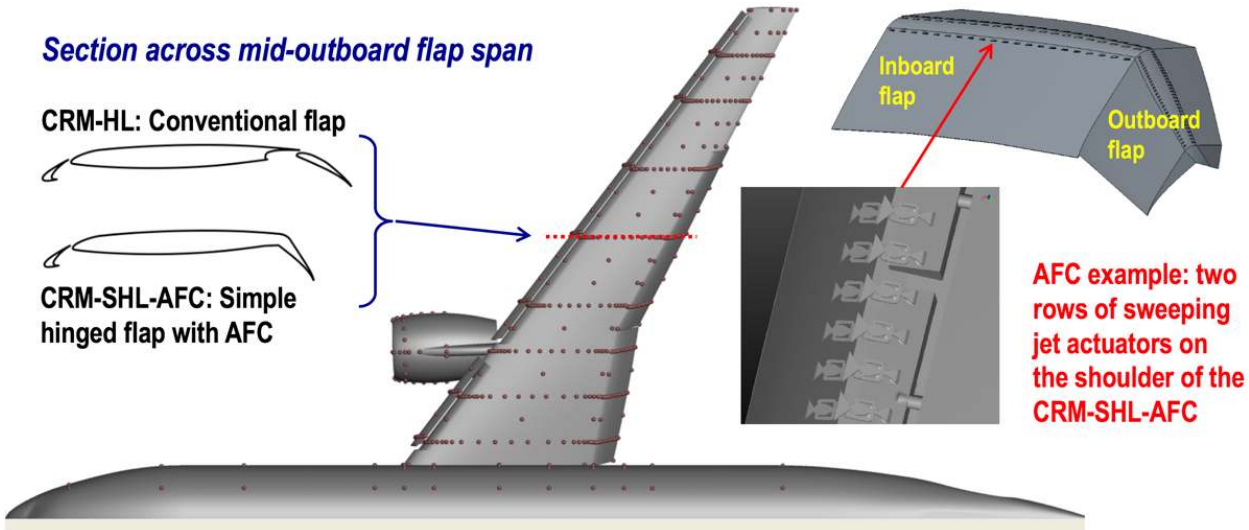

Fig. 4 Schematic of pressure tap locations, cross section of the representative high-lift configurations, and an AFC example.

B. CRM-SHL-AFC Configuration

A simple-hinged flap high-lift configuration was developed and built for AFC implementation. The modular approach provides flexibility and enables the model to be switched between conventional (CRM-HL) and AFC-enabled simple-hinged flap (CRM-SHL-AFC) high-lift configurations. The slats, the WUSS, and the center spar (i.e., almost 70% of the forward cruise chord) remain the same for both high-lift configurations. By using the same conventional slat, the expectation is that the maximum lift should not change significantly. Cross section views of both configurations across the mid-outboard flap location are illustrated in the upper left of Fig. 4 and an example of the sweeping jet actuator AFC installation is shown on the right side of the figure.

The model was used to parametrically explore the effects of different AFC designs on the lift generated by the CRM-SHL-AFC with 50°/55° (inboard/outboard) flap deflections. Ten cavities (or chambers) are located on the shoulder region of the hinged flaps to enable the installation of four interchangeable AFC cartridges on the inboard flap and six on the outboard flap (see Fig 5(a)).

1. AFC Actuators

Two rows of AFC actuators are implemented for enhanced flow-control authority to deal with the strong adverse pressure gradient associated with the 50°/55° flap deflections. Row 1 is the upstream row at the hinge line (forward tangent line) of the simple-hinged flap and Row 2 is downstream, near the aft tangent line of the flap. The three types of AFC devices examined are the Double-Row Sweeping Jets (DRSWJ) [29], the Alternating Pulsed Jets (APJ), and the High Efficiency Low Power (HELP) actuators. These actuator cartridges are illustrated in Fig. 5(b).

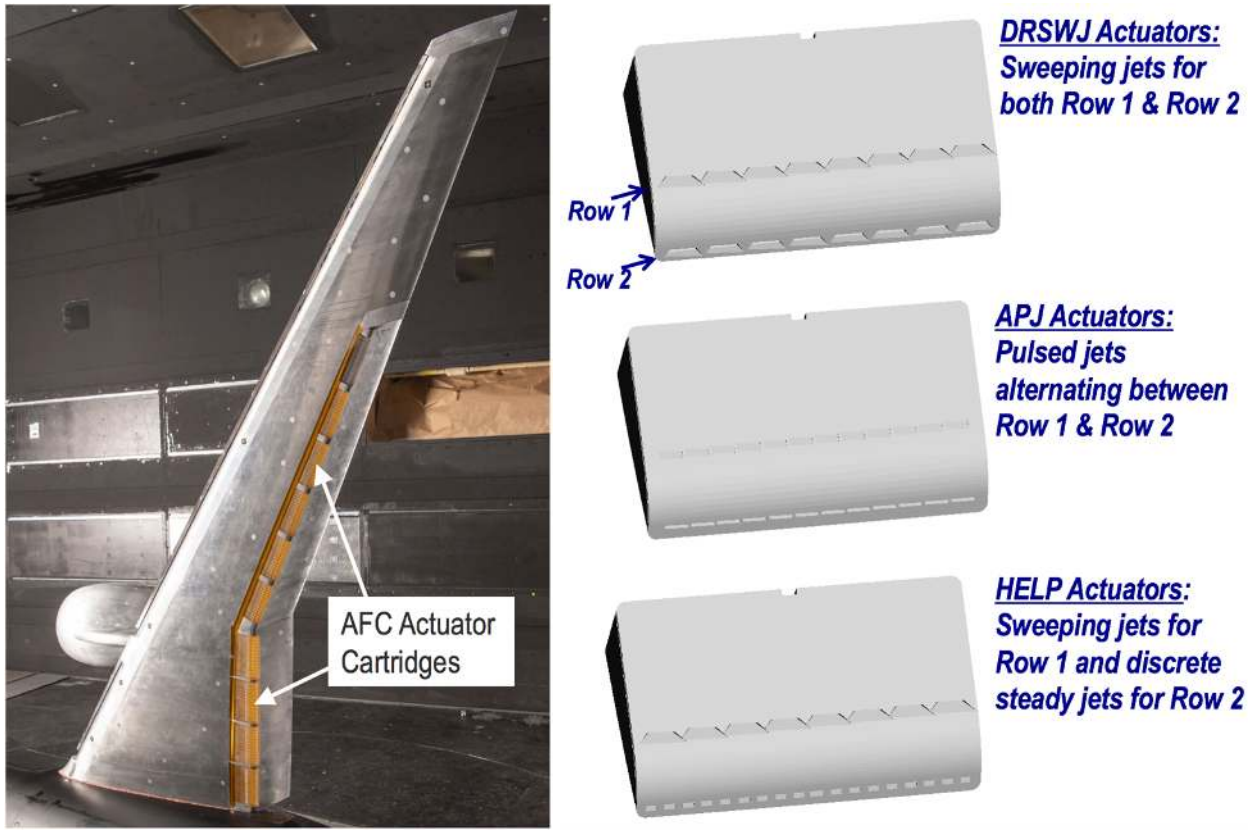

(a) Installation of AFC cartridges. **(b) AFC cartridges.**

Fig. 5 AFC configurations.

The geometrical design of each sweeping jet inside the DRSWJ cartridge is similar to those of the Mod 2 geometry as reported by Melton et al. [21]. The actuators are arranged in-line between the two rows. The inline arrangement and the philosophy of the DRSWJ for AFC is somewhat similar to those reported by DeSalvo, et al. [26]. The APJ actuation is a new actuator design based on the sweeping jet actuator concept that enables exiting jets to pulse alternatingly, but not synchronously, between Row 1 and Row 2. The APJ actuators generate pulsed jets through internal fluid dynamics without the use of any electromechanical moving parts.

The HELP actuation is a new and promising approach that is a combination of unsteady sweeping jet blowing for Row 1 and steady discrete jet blowing for Row 2. The purpose of the HELP design is to enable the sweeping jet actuators of Row 1 to emit a significantly smaller amount of mass flow than that of the discrete jets of Row 2, and therefore, to "precondition the boundary layer" such that the Row 2 actuators can achieve much better flow control authority. The intended goal of the boundary-layer preconditioning is to attenuate the effects of the surface curvature and the adverse pressure gradient at the flap shoulder. The design is also leveraging the synergetic benefit of allowing the two rows of actuators to act together to produce a total aerodynamic lift that is greater than the sum of each row acting individually. The HELP actuation concept is designed to expand the range of flow separation control in the "linear region" of the C_L versus $\dot{m}$ curves as illustrated in Fig. 2, which also makes the HELP actuation highly efficient.

2. AFC Measurements, Parameters, and Control

The total mass flow rate of the AFC system was measured by a Coriolis flowmeter and a thermal mass flowmeter, where the former was only able to measure the flow rate up to ~0.8 lbm/s. Each actuator cartridge's plenum pressure and temperature were measured as well. There are five control valves on a pressure manifold inside the model fuselage and each valve controls a pair of hoses for supplying pressurized air to the ten AFC cartridges. The plenum pressure and mass flow rate for the cartridges could be varied by the control valves and/or by the individual actuators' nozzle exit being physically plugged. The AFC test parameters investigated include actuation type (i.e., DRSWJ, APJ, and HELP actuators), mass flow rate (up to 1.3 lbm/s), nozzle pressure ratio (up to 3), and actuation coverage and spacing.

C. CFD Cooperation

A parallel CFD effort was undertaken to explore the AFC configuration at NASA LaRC, as reported by Vatsa et al. [27,30], using a commercially available Lattice Boltzman solver [31]. This parallel numerical effort has been closely coordinated with the experimental activities and it has played an important role in providing prediction and guidance on the performance of AFC actuators. USM3D and FUN3D flow solvers were also used to simulate the conventional high-lift configuration (CRM-HL) [32]. Parameters examined include various AFC concepts using relatively low pneumatic power. The data obtained for the conventional configuration could be used for the AIAA High-Lift Prediction Workshops as part of its long-term goals for CFD development [33-35]. The CAD for the CRM-HL configuration without the nacelle, wing/fuselage strake, and brackets can be downloaded from the AIAA High-Lift Prediction Workshops website at: https://hiliftpw.larc.nasa.gov/Workshop3/geometries.html [35]. This geometry was also used for the Geometry and Mesh Generation Workshop-1 (GMGW-1) at the AIAA Aviation 2017 Forum. Furthermore, CFD simulations were also performed on the CRM-HL to investigate airframe noise [36] in support of an upcoming aeroacoustic test at the 14x22.

IV. Results and Discussion

A. CRM-HL Results

Aerodynamic performance data of conventional high-lift configuration (CRM-HL) with a 30° slat deflection, a 37° flap deflection, and a nominal slat and flap position setting, as reported by Lacy and Sclafani [10], were acquired as part of the test campaign at the 14x22. The results served as the reference for comparison with those of the CRM-SHL-AFC. The lift performance also provides a target for the CRM-SHL-AFC configuration to achieve. In order to represent a typical modern high-lift system, a wing/fuselage strake (or filler) was installed on the fuselage for all configurations (see left image of Fig. 6(a)). Most of the tests were performed with the engine nacelle attached to the model. However, the installation of a nacelle chine was needed to resolve a prestall lift performance degradation issue for the CRM-HL (see right images of Fig. 6(a)). For completeness of the dataset, the model was also tested with the nacelle removed (see Fig. 6(b)).

Aerodynamic performance plots for the three CRM-HL variants tested — with nacelle, with nacelle and chine, and without nacelle — are shown in Fig. 7. The results are presented in the form of lift curves, drag polar, and pitching moment coefficient (C_m) and lift over drag (L/D) versus α curves. For the CRM-HL variant with nacelle, there was a lift performance degradation between $\alpha = 12°$ and 17° as shown in Fig. 7(a). Flow visualization using minitufts [37] identified that localized flow separation occurred at the trailing edge of the main element, downstream of the nacelle, at several angles of attack prior to stall. It is hypothesized that this flow separation might be due to the interaction of the nacelle wake with an increased adverse pressure gradient near the inboard trailing edge, and perhaps coupling with the wake from the inboard flap fairing, generated at higher α.

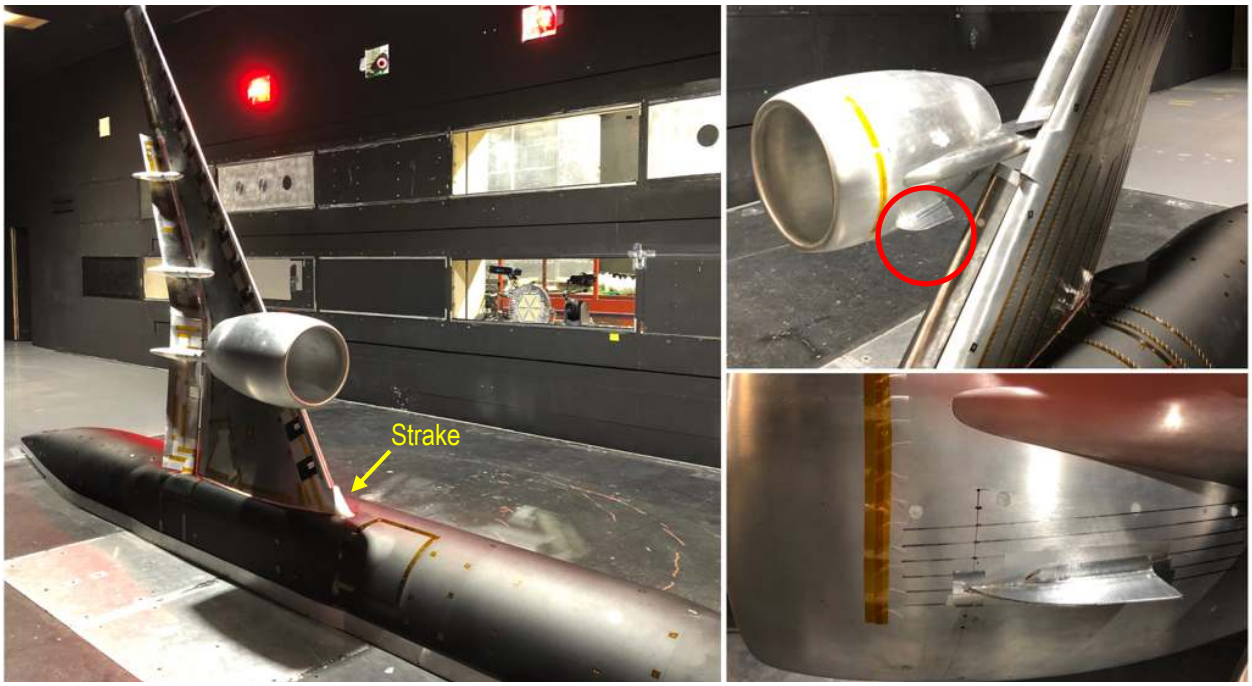

(a) Variants with the engine nacelle (left) and with nacelle chine installed — circled in red (upper right), and close-up view of nacelle chine (lower right).

(b) Variant without the engine nacelle: upper frontal view (left) and lower frontal view (right)

Fig. 6 Photos of the CRM-HL variants installed with conventional flaps.

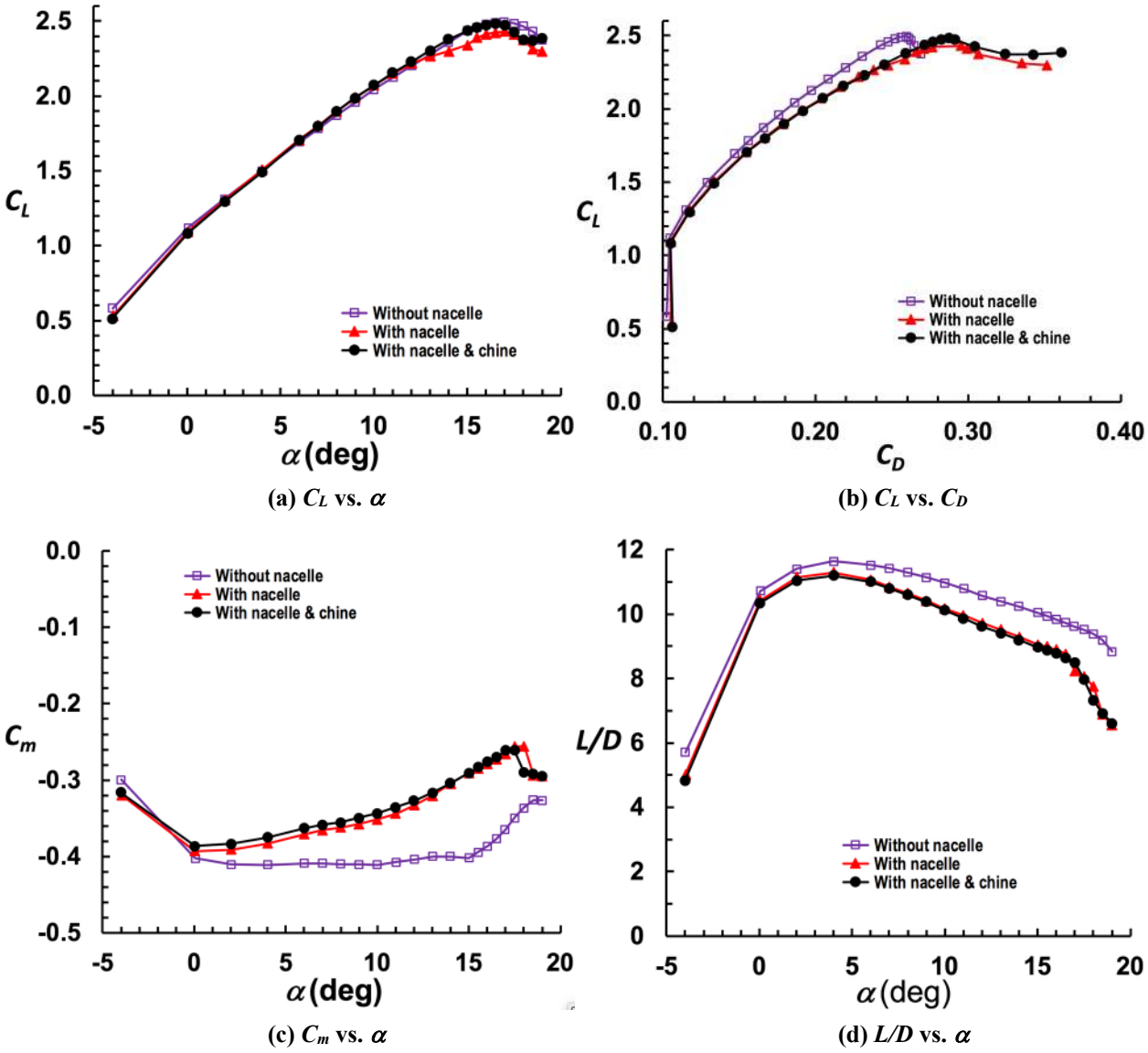

(a) C_L vs. α (b) C_L vs. C_D

(c) C_m vs. α (d) L/D vs. α

Fig. 7 Aerodynamic characteristics of the CRM-HL ($M_\infty = 0.2$).

A nacelle chine has been demonstrated to be effective for flow separation control near maximum lift conditions through wind tunnel testing on a comparable high-lift system (JAXA Standard High-Lift Model) [38,39]. For the current test, a properly placed nacelle chine eliminated the aforementioned localized separation, and therefore provided the necessary lift recovery between $\alpha = 12°$ and 17° as shown in Fig. 7(a). Notice that the results for the variant with nacelle and chine was selected for comparison with the CRM-SHL-AFC cases in the next section of this paper because the prestall lift degradation of the nacelle-only variant is considered unacceptable for practical applications.

As expected, the nacelle-off variant of the CRM-HL produced the lowest drag, the most negative C_m, and the highest L/D for the α range examined, as shown in Figs. 7(b) to 7(d), respectively. The nacelle-off variant had a slightly lower lift around the approach angle of attack than that of the nacelle-on variants as the presence of the nacelle could contribute a small amount of lift (Fig. 7(a)). Figure 7(c) shows that the C_m is negative for all variants tested, which indicates the wing pitches in the nose-down direction that is consistent with typical high-lift wings [40]. The pronounced effect of the nacelle is most clearly seen in the C_m versus α plot. The C_m of the nacelle-off variant is trending with significantly flatter (less positive) slope between $\alpha = 0°$ and 15° compared to the nacelle-on variants. The C_m of the latter are trending with a more positive slope between $\alpha = 0°$ and ~17°. The L/D peaks at about $\alpha = 4°$ for all three variants examined.

The chordwise pressure distributions across the midspan of the inboard flap, y = 27.75 inches, and midspan of the outboard flap, y = 63.8 inches, are shown in Figs. 8 and 9, respectively. They are presented at two key angles of attack (i.e., α = 8° and 16°) for the high-lift design. The first angle, α = 8°, is chosen because it corresponds to a nominal landing approach flight condition for the CRM-HL concept as reported by Hartwich et al. [5]. Figures 8(a) and 9(a) show the comparison for α = 8°, while Figs. 8(b) and 9(b) show the comparison for α = 16°. Notice that the pressure tap location in x is for the deflected coordinates, however, the location specified at y stations of 27.75 inches and 63.8 inches (insert images) is based on the stowed configuration because the deflected y coordinates for the slats and flaps are not in alignment with the freestream direction.

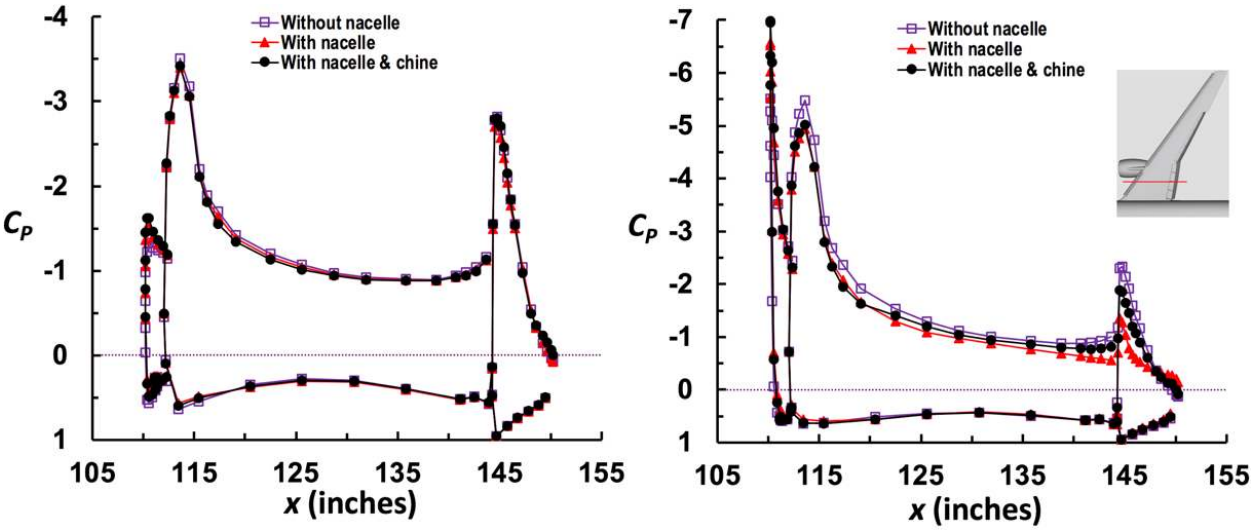

Fig. 8 C_p distributions at y = 27.75" for CRM-HL (M_∞ = 0.2).

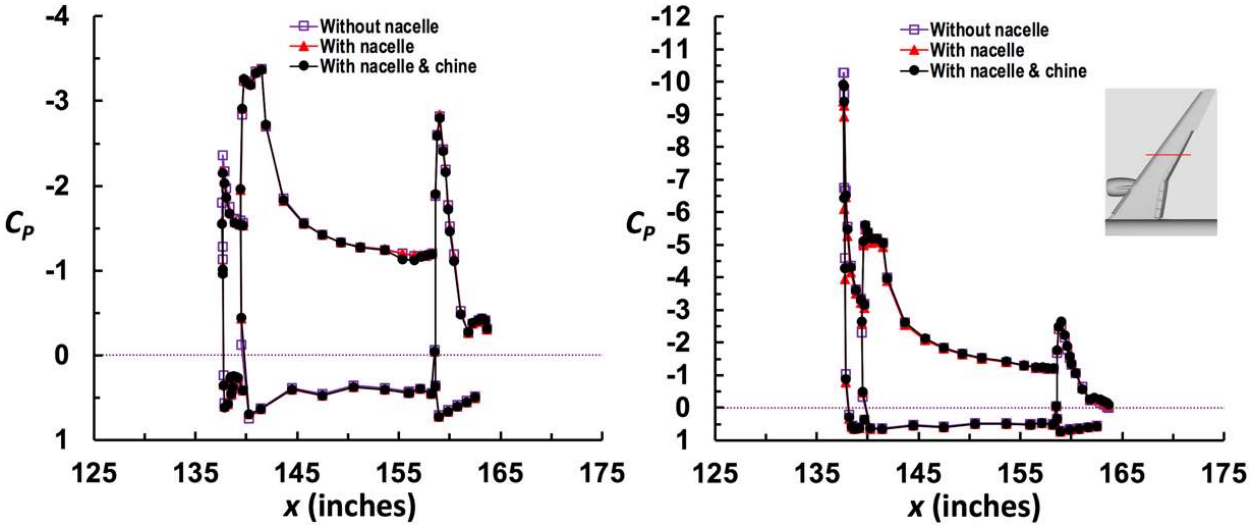

Fig. 9 C_p distributions at y = 63.8" for CRM-HL (M_∞ = 0.2).

For the inboard station (y = 27.75 inches) at α = 8°, the flow is attached around the midspan of inboard flap for all variants tested (Fig. 8(a)), and there is little difference in the pressure distribution between the three CRM-HL variants with conventional Fowler flaps. Near stall (α = 16°), the engine nacelle without chine variant has the lowest suction peak on flap leading edge, with signs of possible flow separation at around 30% flap chord (Fig. 8(b)). Installation of the nacelle chine significantly reduced flow separation on the flap near stall. Figure 8(b) also shows the nacelle-off variant has the highest suction peak around the main wing's leading edge and flap leading edge near stall (α = 16°). The presence of the nacelle resulted in slightly higher suction pressure than that of the nacelle-off case

at this spanwise station (y = 27.75 inches). On the other hand, the presence of the engine nacelle does not seem to significantly affect the pressure distributions for the outboard station (y = 63.8 inches) at both angles of attack, as shown in Figs. 9(a) and 9(b). The difference in the C_p distributions for the three CRM-HL variants (i.e., with the nacelle, with the nacelle plus a chine, and without the nacelle) are negligible.

The suction pressure peak level ($C_p \approx$ -3.7) did not change much between the wing's inboard and outboard leading edges at α = 8° (Figs. 8(a) and 9(a)). However, near stall (α = 16°), the outboard slat carried significantly higher suction pressure than that of the inboard slat (i.e., $C_p \approx$ -10 versus -7, in Fig. 9(b) and 8(b), respectively). Pressure distributions indicated 3D flow separation at ~60% of the outboard flap chord for all CRM-HL variants at both angles of attack (Figs. 9(a) and 9(b)). Minituft flow visualization confirmed the existence 3D separation in this region by showing spanwise flow toward the wing tip [37].

B. CRM-SHL-AFC Results

It was obvious from the start of the AFC testing that the HELP actuation provided strong flow control authority as intended. The synergetic benefit, which results from the two rows actuating together to produce a lift that is greater than the sum of each row actuating individually, is clearly illustrated in the lift curves of Fig. 10. This effect is much more pronounced at higher angles of attack where the adverse pressure gradient is stronger. By design, the sweeping jets of Row 1 discharge a small amount of the mass flow to enable the discrete jets of Row 2 to have greater flow control authority to produce a "Coanda effect boost".

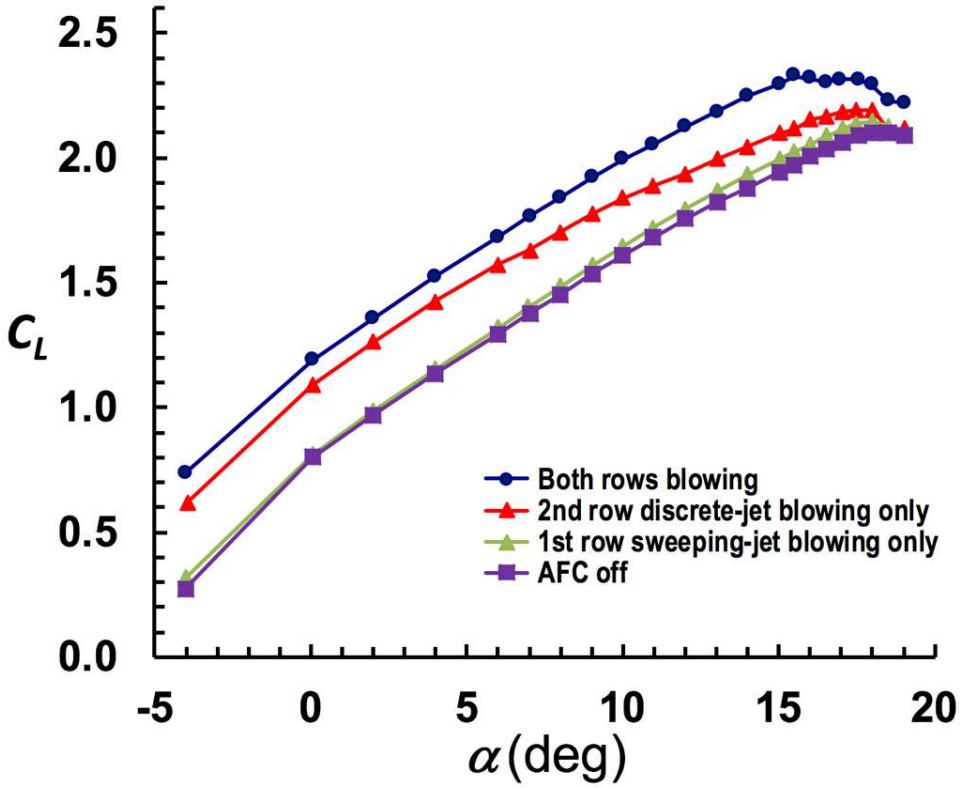

Fig. 10 Synergetic benefit of HELP actuation between 1st and 2nd rows (NPR = 1.5, M_∞ = 0.2).

Similar to Fig. 7, the aerodynamic plots for the four CRM-SHL-AFC cases examined — AFC off (baseline), and the best performer of APJ, DRSWJ, and HELP actuation — are shown in Fig. 11. The results of CRM-HL variant with nacelle and chine is also included in the figure for comparison as it was the one considered acceptable to be used for setting the lift performance goals. Since no prestall lift performance degradation was observed for the CRM-SHL-AFC configuration, no nacelle chine was installed on the model during the AFC portion of the test. Figure 11(a) indicates that the AFC-induced ΔC_L increment was maintained for the entire lift curve, including near the approach angle of attack ($\alpha \approx$ 8°) and near stall ($\alpha \approx$ 16°). The lift curve of the CRM-HL reference case (conventional Fowler flap with nacelle and chine) has a slightly steeper slope compared to the CRM-SHL-AFC configurations, which is likely due to the larger wing area associated with the Fowler flap. The higher slope of the reference case presented extra challenges as the AFC actuators had to work harder to make up for the ΔC_L at higher α. Nevertheless, the lift enhancement produced by the new HELP actuation concept, with nozzle pressure ratio (NPR) 2.4 at all 10 cartridges,

matches or exceeds the lift performance of a conventional Fowler flap (i.e., $\Delta C_L \geq 0.5$), which fulfilled the NASA AATT project goal. The waviness in the lift curve for the HELP actuation was due to the unsteadiness in the supply air control system that was running at the boundary of its operation envelop.

The drag polar, C_m versus α, and L/D versus α curves are shown in Figs. 11(b), 11(c), and 11(d), respectively. The higher flap deflections (50°/55°) of the CRM-SHL-AFC configuration produced higher drag compared to the reference CRM-HL case with a lower flap deflection (37°) as shown in Fig. 11(b). As expected, the HELP actuation produced the highest induced drag (drag due to lift) at higher α.

Figure 11(c) shows that the C_m is negative for all AFC cases tested, and the HELP actuation produced the C_m performance closest to the reference CRM-HL. The AFC off case of the CRM-SHL-AFC has the least amount of the negative C_m. All negative C_m are trending positive between $\alpha = 0°$ and $\alpha \approx 18°$. Compared to the reference CRM-HL, the trends for all AFC cases show a slightly steeper (more positive) slope for $\alpha < 18°$. This is because the Fowler flap of the reference case has a longer moment arm to the moment center than the simple-hinged flap (due to the extension of flap and lower flap deflection), therefore, the suction pressures on flap could produce more nose-down pitching moment (negative C_m) at higher α.

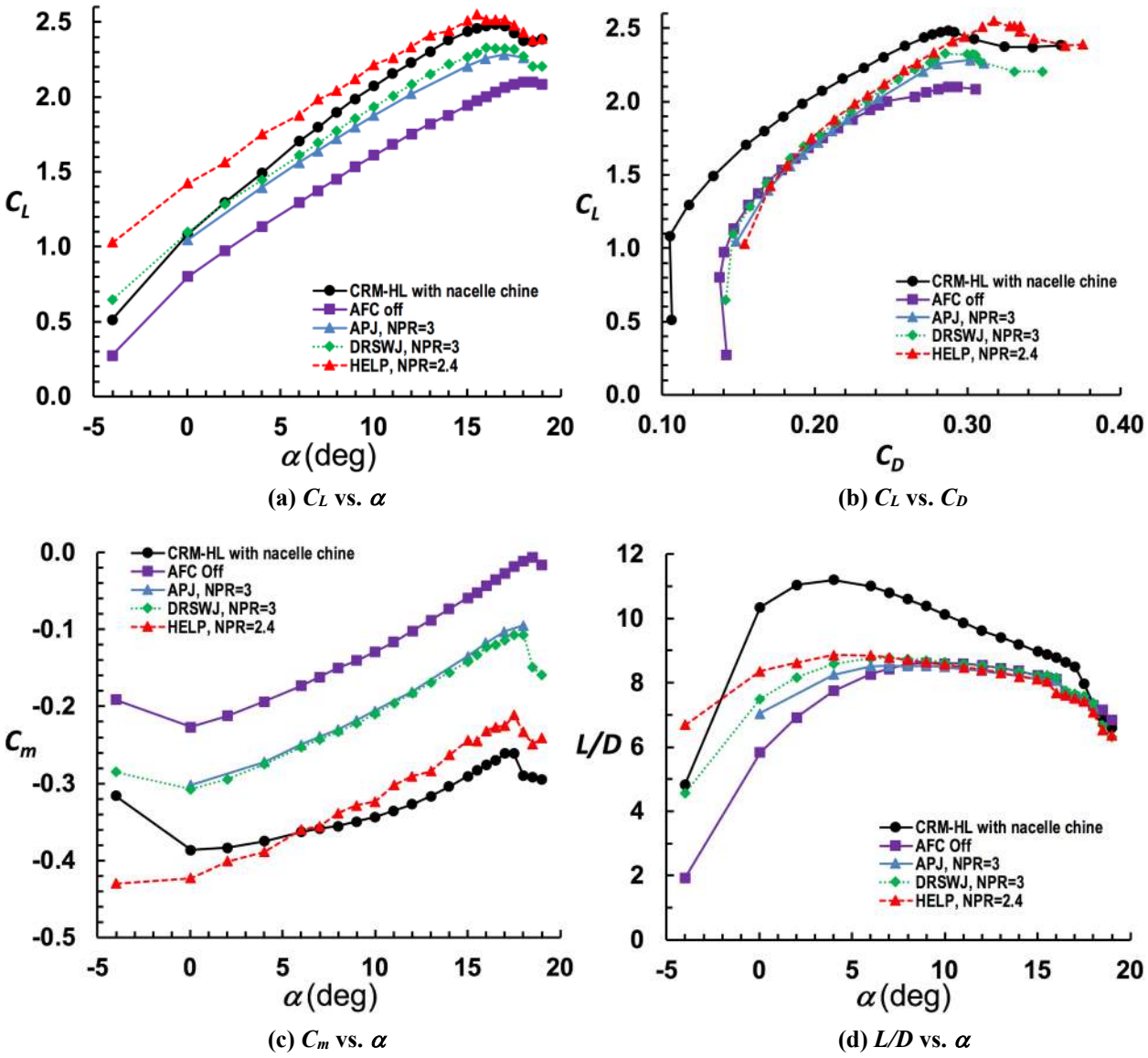

(a) C_L vs. α

(b) C_L vs. C_D

(c) C_m vs. α

(d) L/D vs. α

Fig. 11 Aerodynamics characteristics of the CRM-SHL-AFC and the reference CRM-HL (with nacelle chine), $M_\infty = 0.2$.

The reference CRM-HL generated higher lift-to-drag ratios than all CRM-SHL-AFC cases between $\alpha = 0°$ and stall (Fig 11(d)). However, the variation in *L/D* is smallest for the HELP actuation case. There is little difference in *L/D* with or without AFC for $\alpha > 8°$. The *L/D* peaks at about $\alpha = 4°$ for the conventional and the HELP actuation case. It should be noted that the decrease in *L/D* for the landing configuration could be desirable if significant drag is required to slow down the aircraft.

Similar to Figs. 8 and 9, the chordwise pressure distributions measured at approximately the station across the midspan of the inboard flap (y = 27.75 inches) and the midspan of the outboard flap (y = 63.8 inches) are shown in Figs. 12 and 13, respectively, for the best performer of all CRM-SHL-AFC cases at $\alpha = 8°$ and 16°. The results of reference CRM-HL (variant with nacelle plus chine) are also included in the figure for comparison. Generally speaking, the HELP actuation with NPR = 2.4 achieved the highest suction pressures, and therefore, produced more lift, on the slats and the main wing, whereas the reference CRM-HL (37° conventional flaps) produced higher suction pressures on the flaps, especially on the outboard station.

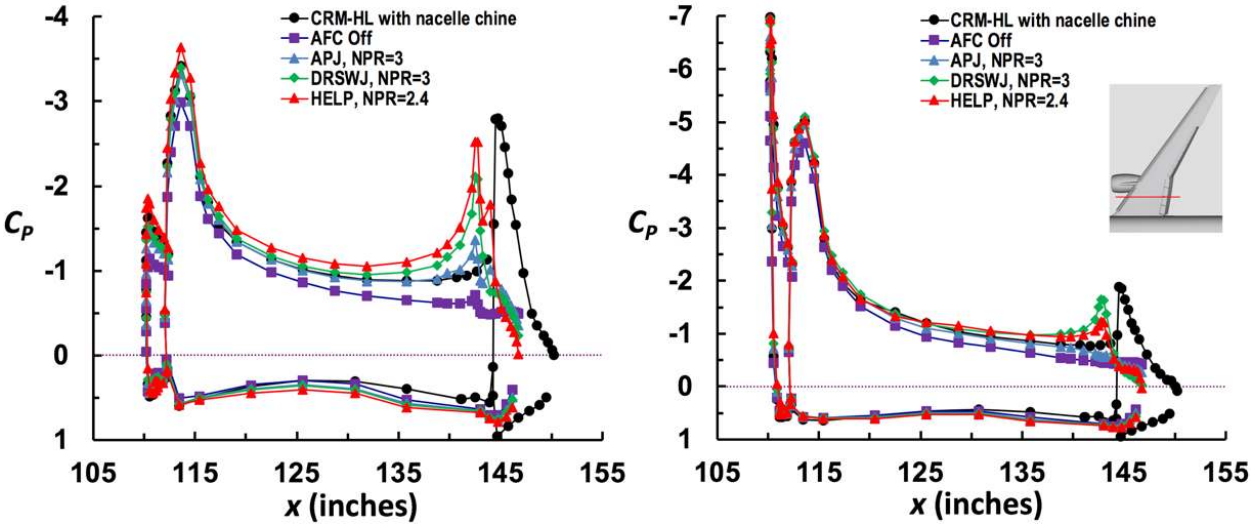

Fig. 12 C_P distributions at y = 27.75" for CRM-SHL-AFC and CRM-HL reference (with nacelle chine), M_∞ = 0.2.

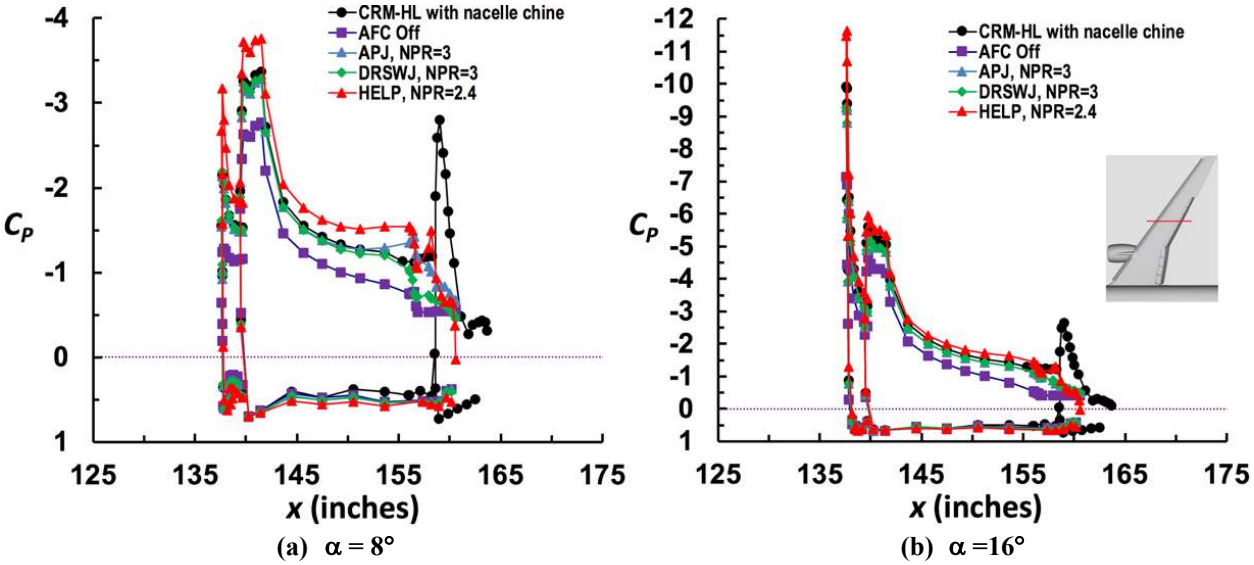

Fig. 13 C_P distributions at y = 63.8" for CRM-SHL-AFC and CRM-HL reference (with nacelle chine), M_∞ = 0.2.

Figures 12 and 13 illustrate that all AFC cases significantly increased the suction pressure on the upper surfaces of the inboard and outboard slats, the main wing, and the inboard and outboard simple-hinged flaps when compared to the AFC off case. For the inboard station (y = 27.75 inches) at α = 8°, the AFC-induced suction pressure increase near the flap hinge line is especially noticeable (Fig. 12(a)). The increase in suction pressure directly resulted in the increase in lift observed for all AFC cases. The DRSWJ actuation with NPR = 3 seems to be more effective on the inboard flap than on the outboard flap, where it produces slightly less than expected suction pressures (Fig. 13(a)).

A maximum suction C_p of approximately -3.7 was achieved on the main wing's leading edge at α = 8° for both spanwise (y) stations (Figs. 12(a) and 13(a)). Perhaps due to the increase in adverse chordwise pressure gradient, substantially higher suction C_p values (approximately -6.9 for inboard and -11.7 for outboard stations) are observed on the slat for the higher angle of attack case (α = 16°) as illustrated in Figs. 12(b) and 13(b). Increased pressure recovery is also observed on the flap surfaces at both angles of attack when using AFC. The pressure increase on the lower (nonactuated) surfaces is minimal at α = 8° and negligible at α = 16°. In summary, applying AFC on the flap shoulder increased the circulation globally, thereby increasing the lift over the entire high-lift wing.

Two key angles of attack for high-lift design, α = 8° for nearing the approach angle of attack and α = 16° for near stall, were selected to streamline the comparison between HELP, DRSWJ, and APJ actuators. Figure 14 shows the effect of nozzle pressure ratio (NPR) on lift for the three AFC actuators. The HELP actuators were the only AFC devices to meet or exceed the targeted lift performance goal, as indicated by the dotted line, which represents the test results of the reference CRM-HL (37° Fowler flap with nacelle and chine). An NPR greater than ~1.8 is needed to achieve the lift enhancement goals for α = 8° and greater than ~2.25 is needed for α = 16°.

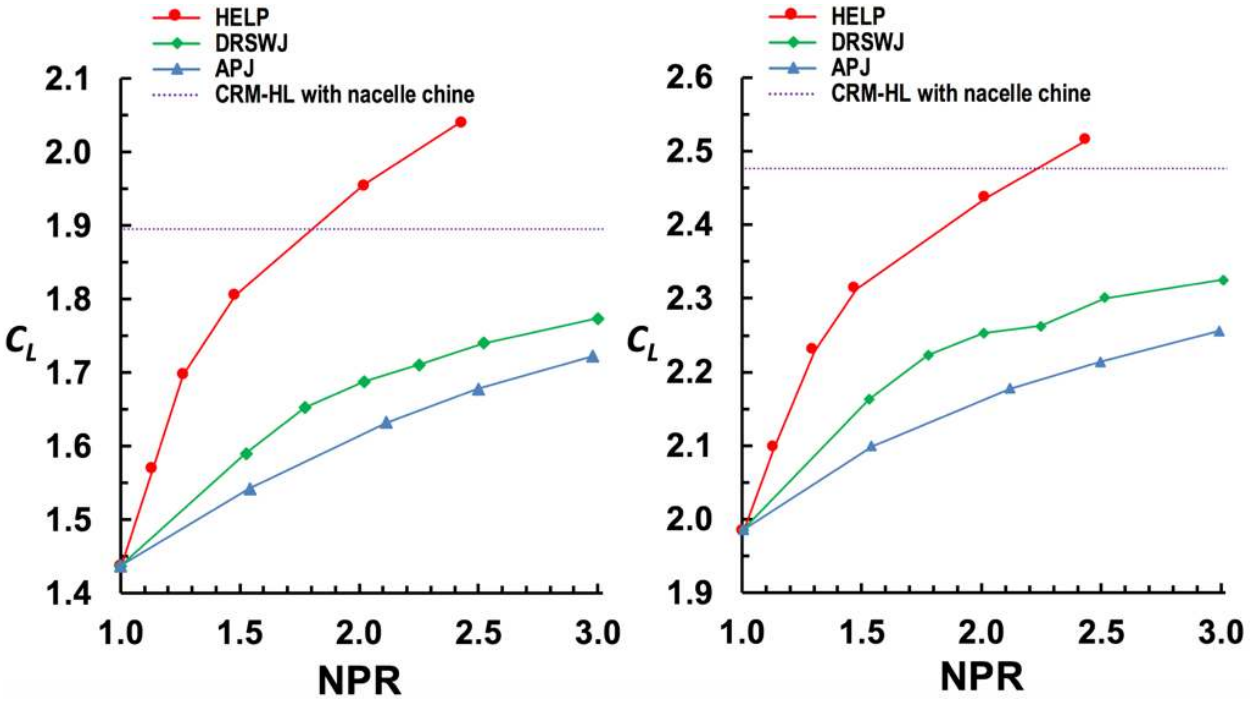

(a) α = 8° **(b) α = 16°**

Fig. 14 C_L versus NPR for DRSWJ, APJ, and HELP actuation (M_∞ = 0.2).

The mass flow rate ($\dot{m}$) is another important AFC parameter to be examined. A complete posttest calibration of the thermal mass flowmeter at three different flow rate ranges (0 to 0.25 lbm/s, 0.8 lbm/s, and 2 lbm/s, respectively) and at various pressures (up to 200 psia) were required to ensure its accuracy. However, only the low- and mid-range calibrations (0 to 0.8 lbm/s) were completed, and the results agree with those of the Coriolis flowmeter, at the time of this writing. Thus, only the mass flow rate results for the α = 8° case (nearing the approach angle of attack) was chosen to provide some preliminary examination of trend and characteristics between HELP, DRSWJ, and APJ actuators (see Fig. 15(a)). Again, the dotted line marks the lift level of the reference CRM-HL, which represents the performance goal. The figure shows that DRSWJ actuators are most effective for $\dot{m}$ < 0.60 lbm/s, whereas the APJ actuators are least effective for $\dot{m}$ > 0.45 lbm/s. However, the HELP actuation concept is extremely effective in extending the range of flow separation control as evident by the a steeper slope for the "linear region" of the C_L versus $\dot{m}$ curves shown in Fig. 15(a). The posttest high-range calibration (0 to 2 lbm/s) of the thermal mass flowmeter, which covers the NPR of 2 and 2.4 for the HELP actuators, is not available at the time of this writing, therefore, the

corresponding $\dot{m}$ values were not plotted in the figure. The actuation efficiency is reversed between HELP and DRSWJ when AFC performance judgement is based solely on $\dot{m}$. Notice that both DRSWJ and APJ results are for actuators operated with an NPR between 2 and 3 (post-choked flows at the nozzle), whereas the HELP results are for an NPR between 1.1 and 1.5 (prechoked flows at the nozzle).

Even without the $\dot{m}$ data corresponding to NPR of 2 and 2.4 for the HELP actuators, it is estimated that a mass flow rate greater than ~0.8 lbm/s (C_Q = 0.0023) is needed for them to achieve the lift enhancement goal of $C_L \approx 1.9$ at $\alpha = 8°$, which corresponds to a momentum coefficient (C_μ) of approximately 0.02.

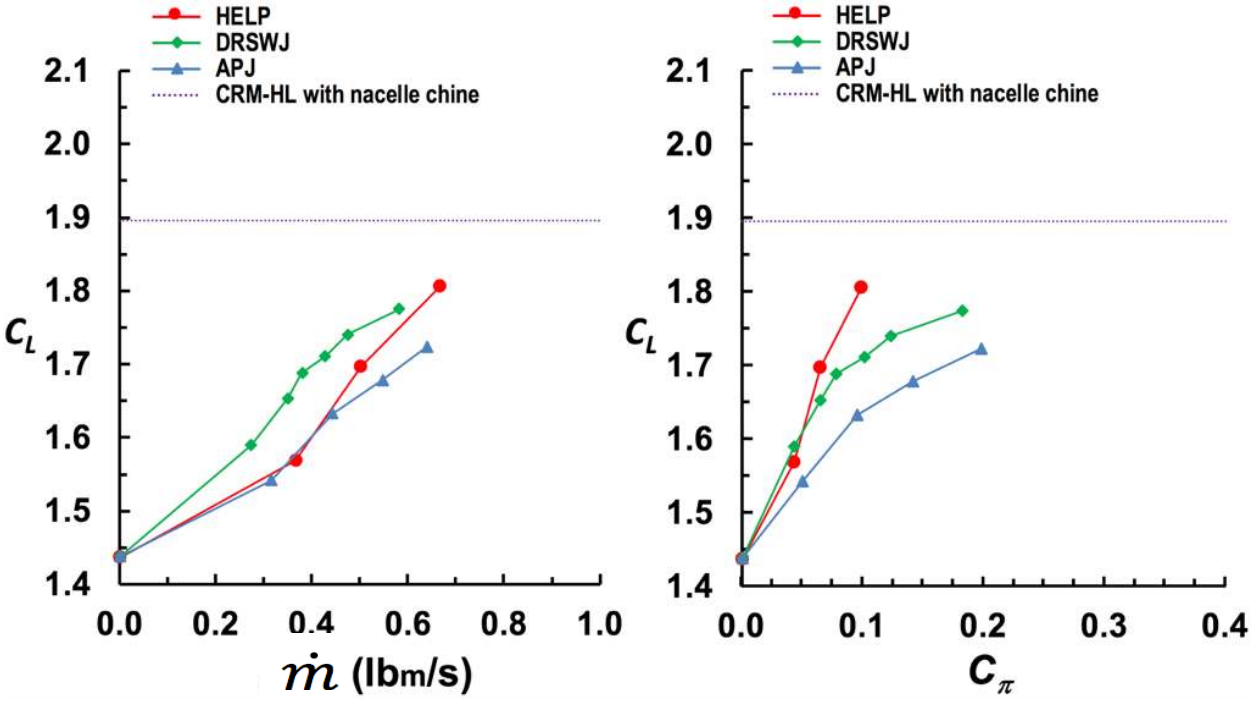

(a) C_L versus $\dot{m}$ **(b) C_L versus C_π**

Fig. 15 C_L versus $\dot{m}$ and C_π for DRSWJ, APJ, and HELP actuation ($\alpha = 8°$, $M_\infty = 0.2$).

Since the supply air pressure (NPR) and the mass flow rate have a contradictory effect on each other, this led to the conclusion that the power coefficient (C_π) is a better parameter to use for judging the performance efficiency of AFC actuators. The power coefficient takes into account both the mass flow rate and the NPR and it is linked to the power usage of a pneumatic-based AFC system as described by Seele et al. [18]. Based on the C_L versus C_π performance at $\alpha = 8°$, AFC using HELP actuators is more effective and efficient than using either DRSWJ or APJ actuators as shown in Fig. 15(b). The HELP actuation has a much steeper slope for C_L versus C_π, which means that it could achieve the C_L that matched the lift performance of a conventional Fowler flap at $\alpha = 8°$ with a relatively low pneumatic power requirement (an estimated C_π of approximately 0.15).

It is believed that the HELP actuation concept can be effective for lift enhancement while minimizing the pneumatic power requirements (mass flow and pressure) for even higher flap deflections and more severe adverse pressure gradients. It should be noted that the HELP actuation concept is still in its infancy as the initial 14x22 test is only the beginning of an ongoing developmental and optimization process for AFC. It is envisioned that using the HELP actuation approach along with pneumatic supply/power provided by a number of microcompressors, engine bypass air, an auxiliary power unit, or any combination thereof may permit the realization of this AFC-enabled high-lift application for future aircraft.

V. Conclusions

A 10%-scale high-lift version of the Common Research Model (CRM-HL) and an AFC-enabled version of the model (CRM-SHL-AFC) were successfully tested at the NASA LaRC 14- by 22-Foot Subsonic Tunnel (14x22). The CRM-HL has a set of 37° inboard and outboard Fowler flaps, whereas the CRM-SHL-AFC has a set of 50° inboard and 55° outboard simple-hinged flaps equipped with integrated modular AFC cartridges on the flap shoulder. Both high-lift configurations share the same 30° slat and engine nacelle.

A prestall lift performance degradation was discovered during the testing of the CRM-HL configuration with nacelle. However, the issue was resolved with a properly placed nacelle chine. The nacelle chine eliminated the localized separation at the trailing edge of the main element downstream from the nacelle, and therefore, provided the necessary lift recovery between α = 12° and 16°. The configuration with nacelle chine was chosen as the representative reference conventional high-lift case for comparison with the CRM-SHL-AFC.

Three new types of AFC devices were investigated on the CRM-SHL-AFC configuration: the Double-Row Sweeping Jets (DRSWJ), the Alternating Pulsed Jets (APJ), and the High Efficiency Low Power (HELP) actuators. These devices were designed to overcome strong adverse pressure gradients while minimizing the mass flow usage. The DRSWJ employed two rows of sweeping jet actuators configured for in-line arrangement. The APJ consisted of exiting jets pulsed alternatingly, but not synchronous, between the upstream and downstream rows. The HELP actuators used a combination of unsteady sweeping jets for the upstream row and steady discrete jets for the downstream row. Nozzle pressure ratio, mass flow consumption, and the power coefficient were used for judging the performance efficiency of the AFC devices. The power coefficient (C_π), which takes account of both supply air pressure and mass flow usage for the AFC actuators, is a useful parameter for judging the actuators' performance efficiency. The AFC-induced ΔC_L enhancement was maintained for the entire lift curve for almost all flow control cases examined. The lift curves of the CRM-HL configurations have a slightly steeper slope compared to the CRM-SHL-AFC configurations, which present extra challenges for AFC at higher angles of attack.

The DRSWJ and the APJ actuators were effective in controlling flow separation, achieving a maximum ΔC_L of ~0.3 and ~0.25, respectively; however, they both fall short of achieving the lift performance of the conventional flap for the pneumatic power examined. The HELP actuation is extremely effective in controlling flow separation in the "linear region" of the lift coefficient (C_L) versus mass flow rate ($\dot{m}$) curves, which also makes it highly efficient. The HELP actuation achieved a targeted lift coefficient increment (ΔC_L) of ~0.50 using a moderate amount of mass flow and supply air pressure. Estimated mass flow rates greater than ~0.8 lbm/s and NPR values greater than ~1.8 (corresponding to $C_\pi \approx 0.15$, C_Q = 0.0023, and C_μ = 0.02) are needed for the HELP actuators to achieve the lift enhancement goal near the approach angle of attack (α = 8°). The CRM-SHL-AFC configuration equipped with HELP actuation was able to match or exceed the lift performance of the reference conventional high-lift configuration (i.e., CRM-HL equipped with a nacelle chine), thus meeting the NASA Advanced Air Transport Technology (AATT) project goal.

The HELP actuation innovation provided a very strong flow control authority via a "Coanda effect boost" as intended. Because the HELP actuation is highly effective in maintaining flow attachment (i.e., enabled the flow to make a hard turn) over a large adverse pressure gradient, there could be other potential aerospace applications for this new technology. These applications may include more efficient vertical and/or short take-off and landing (V/STOL) wings for urban air mobility (UAM) vehicles, flow separation and/or distortion control for compact diffusers upstream of engine-inlets, and bluff-body flow control, just to name a few.

Finally, with the development and the successful testing of the CRM-HL, an "open" geometry high-lift model is now available for R&D efforts for years to come. These efforts can include (but are not limited to) AFC, airframe noise, flow physics, CFD validation, certification by analysis, and icing studies associated with a modern high-lift aircraft.

Acknowledgments

This R&D effort was sponsored by the High Aspect Ratio Wing Subproject under the NASA Advanced Air Transport Technology (AATT) Project. The effort involved many people who provided valuable contributions through their hard work that made a successful test possible. The authors would like to acknowledge and thank all those involved for their great support during the course of this investigation. Some key personnel are as follows.

Model design: Jared Fell (design team lead), Sandy Webb, Miranda Snyder, Christopher Laws, Reggie Kidd, John Mulvaney, Mark Cagle, David Lewis, Nigel Schneider, Dave Castle, Douglas Weber, William Langford, and Ray Rhew, as well as NASA interns Jacob Ganzak and Steven Call.

Model fabrication: Stephen Geissinger, Christopher Mclain, Danny Lovaglio, Robert Andrew, and Thomas Hall.

14x22 air supply system and AFC plumbing: Joe Giuliana.

14x22 managerial staff: Frank Quinto (Facility Manager), Ashley Dittberner (Operation Manager), William Krieger (Facility Safety Head), Joseph Burton (Facility Coordinator).

14x22 Test Engineers: James Byrd (Lead), Abigail Cayton, Jeremy Ulanday, and Samantha Zauber.

14x22 technician and supporting staff:

Lead Technician - Ronald Hunter
Mechanical Technicians - Kyle Deaver (Lead), Joshua Beasley, Marvin Le Gendre, Andrew Sawyer, Cassandra Stevens, and Patricia Christian
Instrumentation Technician - Andrew Harrison, Benjamin Lester, and Neil Coffey
Electrical Technician - Stuart Dale Bennett and Leon Adams
Data System - Andy Boney (Manager), Benjamin Trower, and Charlotte Teague
Facility Equipment Specialist - Karl Maddox
Environmental Coordinator - Joseph Burton, Jr.
High Pressure Air Support - Michael Henshaw and Robert Askew

CRM-HL CFD data: David Lockard and Melissa Rivers
CRM-HL consultation: Douglas Lacy of Boeing Commercial Airplanes.

References

[1] Van Dam, C. P., "The Aerodynamic Design of Multi-Element High-Lift Systems for Transport Airplanes," *Progress in Aerospace Sciences*, Vol. 38, 2002, pp. 101–144. doi: 10.1016/S0376-0421(02)00002-7

[2] Greenblatt, D. and Wygnanski, I. J., "The Control of Flow Separation by Periodic Excitation," *Progress in Aerospace Sciences*, Volume 36, Issue 7, 2000, pp. 487-545. doi: 10.1016/S0376-0421(00)00008-7

[3] Cattafesta III, L. N. and Sheplak, M., "Actuators for Active Flow Control," *Annual Review of Fluid Mechanics*, Vol. 43, Issue 1, August 2010, pp. 247-272. doi:10.1146/annurev-fluid-122109-160634

[4] McLean, J. D., Crouch, J. D., Stoner, R. C., Sakurai, S., Seidel, G. E., Feifel, W. M., and Rush, H. M., "Study of the Application of Separation Control by Unsteady Excitation to Civil Transport Aircraft," NASA/CR 1999–209338, 1999. https://ntrs.nasa.gov/archive/nasa/casi.ntrs.nasa.gov/19990061938.pdf

[5] Hartwich, P. M., Camacho, P. P., El-Gohary, K., Gonzales. A. B., Lawson, E. L., and Shmilovich, A., "System-Level Trade Studies for Transonic Transports with Active Flow Control (AFC) Enhanced High-Lift Systems," *55th AIAA Aerospace Sciences Meeting*, AIAA Paper 2017-0321, 2017. doi: 10.2514/6.2017-0321

[6] Shmilovich, A., Yadlin, Y., Dickey, E. D., Hartwich, P.M., and Khodadoust, A., "Development of an Active Flow Control Technique for an Airplane High-Lift Configuration," *55th AIAA Aerospace Sciences Meeting*, AIAA Paper 2017-0322, 2017. doi: 10.2514/6.2017-0322

[7] Loftin, L. K., "Quest for Performance – The Evolution of Modern Aircraft," NASA SP-468, 1985. https://www.hq.nasa.gov/pao/History/SP-468/ch10-5.htm

[8] Vassberg, J. C., DeHaan, M. A., Rivers, S. M., and Wahls, R. A., "Development of a Common Research Model for Applied CFD Validation Studies," *26th AIAA Applied Aerodynamics Conference*, AIAA Paper 2008-6919, 2008. doi: 10.2514/6.2008-6919

[9] NASA Common Research Model, December 2017. http://commonresearchmodel.larc.nasa.gov

[10] Lacy, D. S. and Sclafani, A. J., "Development of the High Lift Common Research Model (HL-CRM): A Representative High Lift Configuration for Transonic Transports," *54th AIAA Aerospace Sciences Meeting*, AIAA Paper 2016-0308, 2016. doi: 10.2514/6.2016-0308

[11] Lin, J. C., Melton, L. P., Viken, S. A., Andino, M. Y., Koklu, M., Hannon, J. A., and Vatsa, V. N., "High Lift Common Research Model for Wind Tunnel Testing: An Active Flow Control Perspective," *55th AIAA Aerospace Sciences Meeting*, AIAA Paper 2017-0319, 2017. doi: 10.2514/6.2017-0319

[12] Gad-el-Hak, M., "Flow Control," *Applied Mechanics Reviews*, Vol. 42, No. 10, 1989, pp. 261-293. doi: 10.1115/1.3152376

[13] Jones, G. S., Milholen, W. E., II, Chan, D. T., Melton, L. P., Goodliff, S. L., and Cagle, C. M., "A Sweeping Jet Application on a High Reynolds Number Semispan Supercritical Wing Configuration," *35th AIAA Applied Aerodynamics Conference*, AIAA Paper 2017-3044, 2017. doi: 10.2514/6.2017-3044

[14] Milholen, W. E., II, Jones, G. S., Chan, D. T., Goodliff, S. L., Anders, S. G., Melton, L. P., Carter, M. B., Allan, B. G., and Capone, F. J., "Enhancements to the FAST-MAC Circulation Control Model and Recent High-Reynolds Number Testing in the National Transonic Facility," *31st AIAA Applied Aerodynamics Conference*, AIAA Paper 2013-2794, 2013. doi: 10.2514/6.2013-2794

[15] El Sayed, Y., Semaan, R., and Radespiel, R., "Open Loop Control on a Coanda Flap Water Tunnel Model," *35th AIAA Applied Aerodynamics Conference*, AIAA Paper 2017-3247, 2017. doi: 10.2514/6.2017-3247

[16] Gregory, J. W. and Tomac, M. N., "A Review of Fluidic Oscillator Development and Application for Control," *43rd Fluid Dynamics Conference*, AIAA Paper 2013–2474, 2013. doi: 10.2514/6.2013-2474

[17] Seele, R., Tewes, P., Woszidlo, R., McVeigh, M.A., Lucas, N. J., and Wygnanski, I. J., "Discrete Sweeping Jets as Tools for Improving the Performance of the V-22", *AIAA Journal of Aircraft*, Vol. 46, No. 6, pp. 2098-2106, Dec. 2009. doi: 10.2514/1.43663

[18] Seele, R., Graff, E., Lin, J., and Wygnanski, I., "Performance Enhancement of a Vertical Tail Model with Sweeping Jet Actuators," *51st AIAA Aerospace Sciences Meeting*, AIAA Paper 2013-0411, 2013. doi: 10.2514/6.2013-411

[19] Seifert, A., "Evaluation Criteria and Performance Comparison of Actuators for Bluff-Body Flow Control," *32nd AIAA Applied Aerodynamics Conference,* AIAA Paper 2014-2400, 2014. doi: 10.2514/6.2014-2400

[20] Koklu, M., "The Effects of Sweeping Jet Actuator Parameters on Flow Separation Control," *45th AIAA Fluid Dynamics Conference*, AIAA Paper 2015-2485, 2015. doi: 10.2514/6.2015-2485

[21] Melton, L. P., Koklu, M., Andino, M., and Lin, J. C., "Sweeping Jet Optimization Studies," *8th AIAA Flow Control Conference*, AIAA Paper 2016-4233, 2016. doi: 10.2514/6.2016-4233

[22] Ghee, T. A., Raghu, S., and Morgan, A. N., "Sweeping Jet Active Flow Control on a Representative High Performance Military Wing," *2018 AIAA Aerospace Sciences Meeting*, AIAA Paper 2018-1800, 2018. doi: 10.2514/6.2018-1800

[23] Woszidlo, R., Ostermann, F., Schmidt, H.J., "Fundamental Properties of Fluidic Oscillators for Flow Control Applications", *AIAA Journal*, Vol. 57, No. 3, 2019, pp 978-992. doi: 10.2514/1.J056775

[24] Lin, J. C., Whalen, E. A., Andino, M. Y., Graff, E. C., Lacy, D. S., Washburn, A. E., Gharib, M., and Wygnanski, I. J., "Full-Scale Testing of Active Flow Control Applied to a Vertical Tail," *Journal of Aircraft*, 2019, accessed January 29, 2019. doi: http://arc.aiaa.org/doi/abs/10.2514/1.C034907

[25] Whalen, E. A., Shmilovich, A., Spoor, M. A., Tran, J. T., Vijgen, P. M., Lin, J. C., and Andino, M. Y., "Full-scale Flight Demonstration of an Active Flow Control Enhanced Vertical Tail," *8th AIAA Flow Control Conference*, AIAA Paper 2016-3927, 2016. doi: 10.2514/6.2016-3927

[26] DeSalvo, M., Whalen, E., and Glezer, A., "Enhancement of a High-Lift Airfoil using Low-Power Fluidic Actuators," *5th AIAA Flow Control Conference*, AIAA Paper 2010-4248, 2010. doi: 10.2514/6.2010-4248

[27] Vatsa, V. N., Duda, B., Lin, J. C., Melton, L. P., and O'Connell, M., "Numerical Simulation of a Simplified High-Lift CRM Configuration Embedded with Fluidic Actuators," *2018 Applied Aerodynamics Conference*, AIAA Paper No. 2018-3063, 2018. doi: 10.2514/6.2018-3063

[28] Gentry, G. L., Quinto, F. P., Gatlin, G. M., Applin, Z. T. "The Langley 14- by 22-Foot Subsonic Tunnel: Description, Flow Characteristics, and Guide for Users," NASA-TP-3008 September, 1990. https://ntrs.nasa.gov/search.jsp?R=19900018333

[29] Melton, L. P., Lin, J. C., Hannon, J. A., Andino, M. Y., Koklu, M., and Paschal, K. B., "Sweeping Jet Flow Control on the Simplified High-Lift Version of the Common Research Model," accepted for publication at *AIAA AVIATION 2019 Forum*, Dallas, TX, June 17-21, 2019.

[30] Vatsa, V. N., Duda, B., Lin, J. C., Melton, L. P., Lockard, D. P., and O'Connell, M., and Hannon, J. A., "Comparative Study of Active Flow Control Strategies for Lift Enhancement of a Simplified High-Lift Configuration," accepted for publication at *AIAA AVIATION 2019 Forum*, Dallas, TX, June 17-21, 2019.

[31] Fares, E., Wessels, M., Li, Y., Gopalakrishnan, P., Zhang, R., Sun, C., Gopalaswamy, N., Roberts, P., Hoch, J., and Chen, H., "Validation of a Lattice Boltzmann Approach for Transonic and Supersonic Simulations," *52nd AIAA Aerospace Sciences Meeting*, AIAA Paper 2014-0952, 2014. doi: 10.2514/6.2014-0952

[32] Rivers, M., Hunter, C., and Vatsa, V., "Computational Fluid Dynamic Analyses for the High-Lift Common Research Model Using the USM3D and FUN3D Flow Solvers," *55th AIAA Aerospace Sciences Meeting*, AIAA Paper 2017-0320, 2017. doi: 10.2514/6.2017-0320

[33] Rumsey, C. L., Slotnick, J. P., Long, M., Stuever, R. A., and Wayman, T. R., "Summary of the First AIAA CFD High-Lift Prediction Workshop," *Journal of Aircraft*, Vol. 48, No. 6, November-December 2011, pp. 2068-2079. doi: 10.2514/1.C031447

[34] Rumsey, C. L. and Slotnick, J. P., "Overview and Summary of the Second AIAA High-Lift Prediction Workshop," *Journal of Aircraft*, Vol. 52, No. 4, July-August 2015, pp. 1006-1025. doi: 10.2514/1.C032864

[35] Third AIAA CFD High Lift Prediction Workshop, NASA HL-CRM Geometry Files, July 2016. https://hiliftpw.larc.nasa.gov/Workshop3/geometries.html

[36] Lockard, D. P., Choudhari, M. M., Vatsa, V. N., O'Connell, M., Duda, B., and Fares, E., "Noise Simulations of the High-Lift Common Research Model," *23rd AIAA/CEAS Aeroacoustics Conference*, AIAA Paper 2017-3362, 2017. doi: 10.2514/6.2017-3362

[37] Koklu, M., Melton, L. P., Lin, J. C., Hannon, J. A., Andino, M. Y., Paschal, K. B., and Vatsa, V. N., "Surface Flow Visualization of the High-Lift Common Research Model," accepted for publication at *AIAA AVIATION 2019 Forum, Dallas*, TX, June 17-21, 2019.

[38] Kanazaki, M., Yokokawa, Y., Murayama M., Ito, T., Jeong, S., and Yamamoto, K., "Efficient Design Exploration of Nacelle Chine Installation in Wind Tunnel Testing," *46th AIAA Aerospace Sciences Meeting*, AIAA Paper 2008-155, 2008. doi: 10.2514/6.2008-155

[39] Kato, H., Watanabe, S., Murayama, M., Yokokawa Y., and Ito, T., "PIV Investigation of Nacelle Chine Effects on High-Lift System Performance," AIAA Paper 2008-240, 2008. doi: 10.2514/6.2008-240

[40] Gatlin, G. M. and McGhee, R. J., "Experimental Investigation of Semispan Model Testing Techniques," *Journal of Aircraft*, Vol. 34, No. 4, July-August 1997, pp. 500-505. doi: 10.2514/2.2219